



Modified Unsteady Vortex-Lattice Method to Study Flapping Wings in Hover Flight

Bruno A. Roccia,* Sergio Preidikman,† and Julio C. Massa‡
National University of Córdoba, 5000 Córdoba, Argentina

and

Dean T. Mook§

Virginia Polytechnic Institute and State University, Blacksburg, Virginia 24061

DOI: 10.2514/1.J052262

A numerical-simulation tool is developed that is well suited for modeling the unsteady nonlinear aerodynamics of flying insects and small birds as well as biologically inspired flapping-wing micro air vehicles. The present numerical model is an extension of the widely used three-dimensional general unsteady vortex-lattice model and provides an attractive compromise between computational cost and fidelity. Moreover, it is ideally suited to be combined with computational structural dynamics to provide aeroelastic analyses. The present numerical results for a twisting, flapping wing with neither leading-edge nor wing-tip separations are in close agreement with the results obtained in previous studies with the Euler equations and a vortex-lattice method. The present results for unsteady lift, mean lift, and frequency content of the force are in good agreement with experimental data for the robofly apparatus. The actual wing motion of a hovering *Drosophila* is used to compute the flowfield and predict the lift force. The downward motion of the fluid particles revealed in the graphics of the calculated wake indicates the presence of lift. Moreover, the calculated mean lift is in close agreement with the weight of a *Drosophila*. The results presented in this paper definitely show that the interaction between vortices is the main feature that allows insects to generate enough lift to stay aloft. The present results warrant the use of this general version of the unsteady vortex-lattice method for future studies.

Nomenclature

AR	= aspect ratio
$\mathbf{A}(t)$	= aerodynamic influence matrix
c, c_{\max}	= wing chord and maximum chord length
C_L	= lift coefficient
L, \bar{L}	= lift force and mean lift force
L_b	= body length
$\hat{\mathbf{n}}$	= unit vector normal to the body surface
n_f, T_f	= flapping frequency and flapping period
$p(\mathbf{r}, t), p_\infty$	= unknown pressure and pressure far away from the body
R	= wing length
Re	= Reynolds number
\mathbf{r}	= position vector
$\mathbf{R}_{\text{node}}, \mathbf{V}_{\text{node}}$	= position and velocity of an aerodynamic-panel corner
t, t^*	= dimensional and nondimensional time
$\mathbf{V}(\mathbf{r}, t)$	= velocity field
$\mathbf{V}_p, \mathbf{V}_\infty$	= body-surface velocity and freestream velocity
α_e, α_c	= effective angle of attack and reference angle of attack
$\Gamma(t)$	= circulation associated to a finite segment of a vortex line
δ	= cutoff radius
$\eta(t)$	= twisting angle

$\nu_{\text{air}}, \nu_{\text{oil}}$	= air kinematic viscosity and oil kinematic viscosity
ρ, ρ_{oil}	= constant density and density of the oil used in the robofly experiment
χ, β	= body angle and stroke plane angle
Φ	= wing beating amplitude
$\phi(t), \theta(t), \psi(t)$	= stroke position angle, stroke deviation angle, and rotation angle
$\Psi(\mathbf{r}, t)$	= potential velocity
Ω	= vorticity field
ω	= finite vortex segment

I. Introduction

SINCE several years ago, the scientific community has specifically focused on the study of flying insects and small birds in order to inspire the development of micro aerial vehicles (MAVs) with flapping wings. Nevertheless, there are still major technical barriers to be overcome, such as to definitely understand how these flying creatures generate sufficient aerodynamic forces in order to propel themselves and stay aloft. There are a number of experimental investigations on the aerodynamic of insect flight, many of them carried out by Dickinson and Götz [1] and Ellington [2], Van den Berg and Ellington [3], and Ellington et al. [4], which provide comprehensive studies of the unsteady aerodynamic mechanisms used by flying insects and small birds. From a numerical point of view, clearly, the best approach to understanding flight at small scales would be to solve for the complete viscous flow around the insect or bird. However, solutions of the full Navier–Stokes equations for three-dimensional (3-D), unsteady flowfields having boundaries experiencing relatively large complicated motions are challenging to solve. Significant computational difficulties and cost associated to the use of models based on computational fluid dynamics (CFD) techniques have led to the utilization of a large variety of aerodynamic models to study the natural flight.

Vest and Katz used a panel method to numerically model flapping-wing aerodynamics [5]. Ramamurti and Sandberg [6] employed the Euler equations to compute the 3-D flow around a fly's wing and then compared their numerical results with the experimental results obtained by Dickinson et al. [7], finding good agreement. Ansari et al. [8,9] extended the work of Von Karman and Sears [10] to include the

Received 6 August 2012; revision received 13 May 2013; accepted for publication 16 May 2013; published online 13 September 2013. Copyright © 2013 by the American Institute of Aeronautics and Astronautics, Inc. All rights reserved. Copies of this paper may be made for personal or internal use, on condition that the copier pay the \$10.00 per-copy fee to the Copyright Clearance Center, Inc., 222 Rosewood Drive, Danvers, MA 01923; include the code 1533-385X/13 and \$10.00 in correspondence with the CCC.

*Assistant Professor, Structures Department, School of Exact, Physical, and Natural Sciences; bruno.roccia@gmail.com.

†Professor, Structures Department, School of Exact, Physical, and Natural Sciences. Member AIAA.

‡Professor, Structures Department, School of Exact, Physical, and Natural Sciences.

§Waldo Harrison Professor Emeritus, Department of Engineering Science and Mechanics (MC 0219). Associate Fellow AIAA.

leading-edge vortex (LEV) effects by shedding vortices from both of the leading and trailing edges. They derived two nonlinear integral equations for the shed wake and leading-edge vortices. Because of the computational cost associated with this formulation, its use in aerodynamic analysis, sensitivity analysis, and dynamic and control is still limited. Ansari et al. also compared their results with those obtained by Dickinson.

Liu and Kawachi [11] and Liu et al. [12] used a CFD model to study the unsteady aerodynamics of the flapping wings of a hovering hawkmoth (*manduca sexta*). They detected a LEV with axial flow during translational motions consistent with the results observed by Ellington et al. [4]. Sun and Tang [13,14] used a time-dependent body-conforming grid to obtain a 3-D solution for the flow around a fruit-fly wing. They confirmed the results observed by Dickinson [15] on force enhancement influenced by the timing of the wing's rotation while translating. Sun and Du [16] performed the same study on a wide range of eight insects. Sun and Wu [17] solved the Navier–Stokes equations on the wing and body of the fruit fly in forward flight. Tang et al. [18] used a CFD code to investigate the wake-capture mechanism during hovering flight. The computational results of Tang and coauthors identified a secondary lift peak after the stroke reversal while hovering, also in good agreement with the results observed by Dickinson et al. [7]. Also, it is worthwhile to look at the model of DeLaurier [19] for forward flight. This model aimed at checking the aerodynamic calculations of the Pterosaur developed by AeroVironment, and it included low-fidelity representations of the 3-D unsteady effects, friction effects, partial leading-edge suction, and a poststall behavior.

Currently, the use of unsteady vortex-lattice methods (UVLMs) has been gaining ground in the study of nonstationary problems in which free-wake methods become a necessity because of geometric complexity, such as flapping-wing kinematics, morphing wings, and rotorcraft, among others. The pioneering works in the development of UVLMs were carried out by Belotserkovskii [20], Rehbach [21], and researchers at Virginia Tech [22,23] and Technion [24,25]. Possibly the most comprehensive description of UVLM was given by Katz and Plotkin [26]. Related to flapping-wing aerodynamics, five terms can be identified as the main contributors to flow quantities during hover. They include the effects due to the wing's translation and rotation, the LEV, wake capture, viscosity, and added mass. UVLMs capture all except the viscous and the LEV effects. As shown by the experiments of Dickinson et al. [1,7], the viscous effects for the range of Reynolds numbers (75–4000) of hovering MAVs/insects can be neglected, which makes the use of the UVLM suitable for the study of flapping-wing aerodynamics.

Fritz and Long [27] implemented the UVLM using object-oriented computing techniques to model the oscillating plunging, pitching, twisting, and flapping motions of a finite-aspect-ratio wing. The work carried out by Fritz and Long showed that the method is capable of

accurately simulating many of the features of complex flapping-wing flight, although their model does not take into account the leading-edge-vortex phenomenon. Stanford and Beran [28] also used UVLMs to consider the design optimization of a flapping wing in forward flight with active shape morphing, aimed at maximizing propulsive efficiency under lift and thrust constraints. Ghommem et al. [29] tackled the same problem using global and hybrid optimization techniques. Ghommem used a two-dimensional (2-D) version of the UVLM to obtain the hovering kinematics that minimizes the required aerodynamic power under a lift constraint. Willis et al. [30] presented a simulation tool, FastAero, which uses a panel method along with an approach based on vortex particles to represent the wake shed from the wing's trailing edge. The approach used by Willis and coworkers was demonstrated to be efficient and accurate to study a variety of problems involving unsteady flows and highly flexible lifting surfaces undergoing complex motions. Eldredge [31] also used a method based on vortex particles to carry out numerical simulations of the fluid dynamics of 2-D rigid-body motion, and he showed its utility for investigating biological locomotion: a flapping elliptical wing with hovering insect kinematics, with good agreement of forces with previous results reported by Wang et al. [32] and a three-linkage “fish” undergoing undulating motion. For more details on the aerodynamics of flapping flight, the reader is referred to [33–37]. The different models previously discussed in the literature review are summarized in Table 1.

In this paper, we significantly extend the capability of UVLMs in order to study the aerodynamics of a fruit fly (*Drosophila Melanogaster*) by including 1) leading-edge separation, 2) the insect's body structure (head, thorax, and abdomen), and 3) different kinematic patterns. The present aerodynamic model takes into account all possible aerodynamic interference and allows us to predict 1) the flowfield around an insect's body and wings, 2) the spatial–temporal vorticity distribution attached to the insect's body and wings, 3) the vorticity distribution in the wakes emitted from the sharp edges of the wings, 4) the position and shape of these wakes, and 5) the unsteady aerodynamic loads acting on the wings.

Because the UVLM models inviscid flow, it is not capable to predict Reynolds-number effects, and therefore, the location of separation, such as along the wing tips, trailing edges, and leading edges, as well as other possibilities, must be input by the programmer. In this work, the leading-edge separation was taken into account by means of a simply scheme based upon an on/off mechanism.

To the best of the authors' knowledge, an aerodynamic study of flapping wings in hover motion by means of an UVLM involving a free deforming wake in the time domain, time-dependent geometries and largely attached flows is unavailable in the literature, and it is the focus of the present work. Furthermore, it must be highlighted that the model developed in this work provides an attractive compromise between computational cost and fidelity.

Table 1 Summary table of numerical aerodynamic models

Authors	Model	Application
Vest and Katz [5]	Panel method (3-D)	Flapping wing at high advanced ratios ($J = 4.31$) and high-frequency flapping flight ($J = 0.76$)
Ramamurti and Sandberg [6]	Incompressible Navier–Stokes equations (3-D)	Fruit fly
Ansari et al. [8,9]	UVLM (2-D), extended to 3-D by means of the blade-element theory (radial chords)	Insectlike flapping wing
Liu et al. [11,12]	Incompressible unsteady Navier–Stokes equations (3-D)	Manduca Sexta flight
Sun and Tang [13,14]	Incompressible unsteady Navier–Stokes equations (3-D)	Fruit fly
Sun and Du [16]	Sun and Tang model [13,14]	Fruit fly, crane fly, ladybird, hawkmoth, hoverfly, dronefly, honey bee, and bumble bee
Sun and Wu [17]	Sun and Tang model [13,14]	Fruit fly
Tang et al. [18]	Incompressible unsteady Navier–Stokes equations (2-D)	Elliptic airfoil–water treading, hovering mode, and normal hovering mode
DeLaurier [19]	A modified strip theory	Pterosaur developed by AeroVironment
Fritz and Long [27]	UVLM (3-D)	Finite-aspect-ratio wing undergoing oscillating plunging, pitching, twisting, and flapping motions
Stanford and Beran [28]	UVLM (3-D)	Optimization of morphing wings
Ghommem et al. [29]	UVLM (3-D)	Global optimization of morphing wings
Willis et al. [30]	Panel method combined with vortex particles (3-D)	Morphing wings/flapping wings
Eldredge [31]	Vortex-particle method (2-D)	Biological locomotion

The remainder of this work is organized as follows. A brief introduction to the natural flight of insects, including the unsteady aerodynamic mechanisms that characterize the flight at small scales, is given. This is followed by a general description of both the insect-wing kinematic model and the UVLM, as well as a detailed explanation of the leading-edge separation model. Next, the aerodynamic model is validated by comparing numerical results with those obtained by Stanford and Beran [28] and Neef and Hummel [38] and, finally, with the force data reported by Dickinson et al. [7]. Then, the numerical results for a fruit fly in hover are presented. The work concludes stating the limitations of the model and how these issues can be addressed in order to extend its applicability.

II. Model Description

A. Model Insect

The insect model adopted in this paper to study the aerodynamics of flapping wings corresponds to a fruit fly (*Drosophila Melanogaster*). The model is based on the work of Markow and O'Grady to preserve certain morphological parameters such as wing length R , body length L_b , maximum chord length c_{\max} , and geometry of the wing and the insect's body (see Fig. 1) [39].

For simplicity, each part of the insect's body (head, thorax, and abdomen) was modeled as a surface of revolution. This model was entirely implemented in MATLAB® using a parametric technique that allows, easily and interactively, the construction of computational models of insects of different sizes while preserving the creature's proportions. The surfaces of revolution that define the insect's body as well as the surfaces that model the insect's wings were discretized using simple, nonplanar, quadrilateral four-node elements. This discretization is explained in Sec. II.C.2.

B. Kinematical Model

To describe the trajectory of any arbitrary point on the insect's wing, we used four reference systems, including 1) an inertial or Newtonian reference system N , 2) a body-fixed system T located at the mass center of the thorax, 3) a reference system fixed to the stroke plane Z , and 4) two reference systems fixed to each wing root in order to facilitate its special discretization B for the left wing and A for the right wing (see Fig. 2).

The orientation of the insect's body is exclusively affected by a change in the body angle χ and is obtained by means of one rotation (1 – rotation) of the reference frame T .

The orientation of the stroke plane with respect to the inertial frame N is accomplished in two stages. First, the stroke plane is positioned perpendicularly to the longitudinal axis of the insect by means of the body angle, and next, the stroke plane is orientated with respect to an axis perpendicular to the longitudinal axis of the creature by means of the stroke-plane angle β .

The wing's orientation relative to the stroke plane is defined by three angles, including 1) the stroke position angle $\phi(t)$; 2) the stroke

deviation angle $\theta(t)$; and 3) the rotation angle about the wing's longitudinal axis, $\psi(t)$. We define the wing's orientation with the sequence of rotations (1-3-2) given by the Euler angles $\phi(t)$, $\theta(t)$, and $\psi(t)$, respectively.

Figure 2 shows the definition of the angles mentioned in the preceding paragraph. The stroke position angle is formed by the projection of the longitudinal axis of the wing on the stroke plane and the unit vector \hat{z}_1 and is positive when the wing is in the ventral position. The stroke deviation angle is defined as the angle formed by the longitudinal axis of the wing and the stroke plane and is considered positive when the wings are above the stroke plane. The rotation angle is measured on a plane Π , which has an orientation in 3-D space that is always normal to the unit vector \hat{b}_2 fixed to the wing; it is defined as the angle formed by the wing's chord and the straight line EE' , which is fixed to the Π plane and coincides with the direction of the unit vector \hat{b}_1 at $t = 0$. This angle is positive in a downstroke.

The reader may consult reference [40] for a detailed description of the stroke parameters and a full mathematical formulation of the flapping-wing kinematics.

C. Aerodynamic Model

In this paper, we present an enlarged and modified version of the UVLM. The enlarged method can be applied to 3-D lifting and nonlifting flows. It is general in the sense that the surface of the body may undergo any time-dependent deformation while the body executes any type of maneuver in the space surrounded by moving air. The flow around the body (meaning the insect's body and wings) is assumed to be irrotational and incompressible over the entire flowfield, except next to the solid boundaries of the body and in the wake. This approach allows us to consider nonlinear and unsteady aerodynamic effects associated with large angles of attack and static deformations. The UVLM also allows us to take all possible aerodynamic interferences into account as well as to estimate the spatial-temporal vorticity distribution attached to the body's surface, the vorticity distribution in, as well as the position and shape of, the wakes shed from the sharp edges of the wings.

As a result of the relative motion between the body and the fluid, vorticity is generated in the fluid in a thin region adjoining the surface of the body (the boundary layer). This vorticity is shed from the sharp edges and forms the wake. We consider both the boundary layers and the wakes to be sheets of vorticity.

The bound-vortex sheet represents the boundary layer on the surface the body, and its position is specified (i.e., it adheres to, and moves with, the body, not with the fluid particles). For the case of thin wings, the vortex sheets on the upper and lower surfaces are merged into a single surface along the camber line. On the other hand, the positions of the free-vortex sheets representing the wakes are not specified a priori; they are allowed to deform freely until they assume force-free positions as determined by the solution. The two types of vortex sheets are joined along the sharp edges where separation

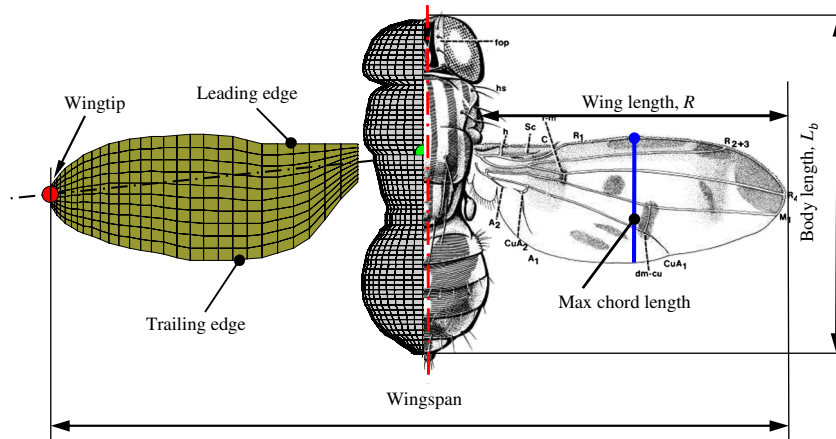


Fig. 1 Geometric model of an insect and the definitions of morphological parameters.

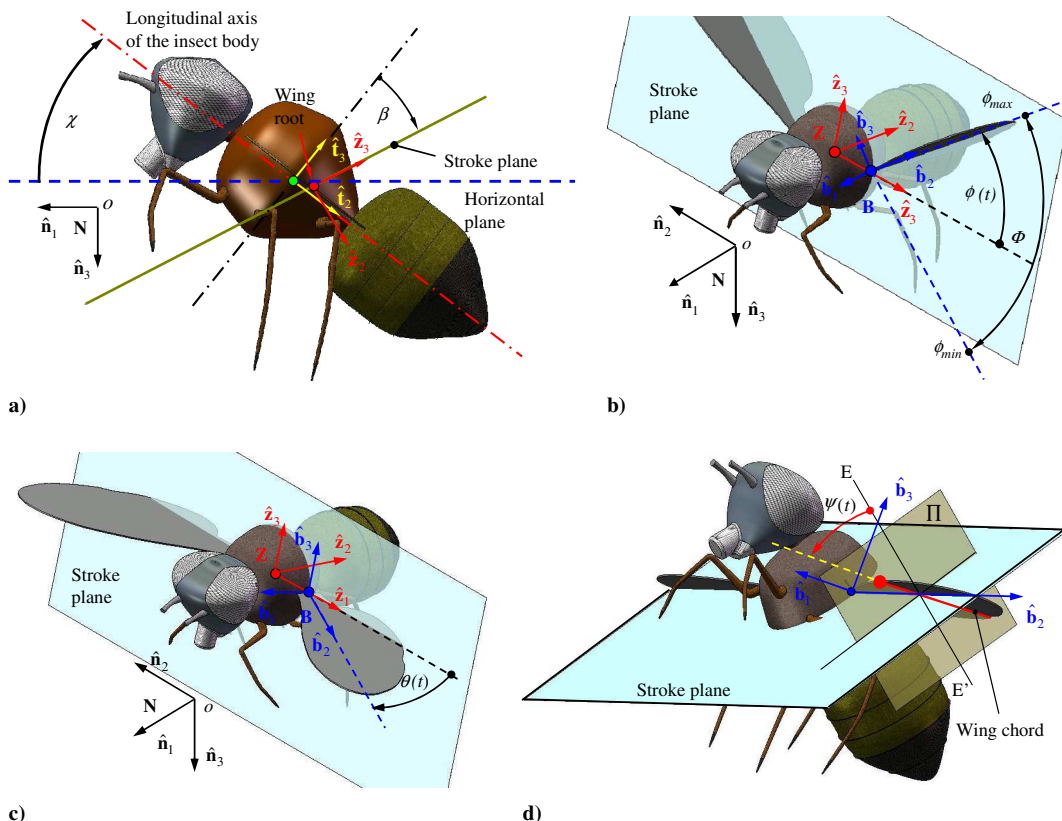


Fig. 2 Stroke parameters definitions: a) body angle and stroke plane angle, b) stroke position angle, c) stroke deviation angle, and d) rotation angle.

occurs; the same edges in which the Kutta condition is imposed in a steady flow.

There is a kinematic relationship between vorticity and velocity such that, if there is vorticity anywhere in the flowfield, then there is velocity associated with it everywhere in the flowfield; the velocity decays with distance from the vorticity. The vorticity in the wake at any given time was generated on and shed from the wings at an earlier time; the velocity associated with this wake vorticity affects the flow near the wing and therefore the loads on the wings. As a result, the aerodynamic loads depend on the history of motion, and the wake is the *historian*. As the vorticity in the wake is transported downstream, its influence decreases, and therefore, the historian has a fading memory. Fading memory is a very good thing because it means that the part of the wake to be taken into account need not be very long.

Ramamurti and Sandberg [6] studied the effects of viscosity on unsteady flow surrounding a 3-D *Drosophila* wing undergoing flapping motion. They showed that these effects are minimal and that lift and drag forces are dominated by inertial effects. The chord-based Reynolds number that characterizes insect flight is relatively low, and so the question naturally arises, can UVLM be reliably used to predict the aerodynamic loads on flapping wings? We provide the answer here.

1. Mathematical Formulation

The continuity equation for incompressible flow governs the velocity field $V(r, t)$:

$$\text{Div}V(r, t) = 0 \tag{1}$$

The time dependence is introduced by the moving boundary. The vorticity field Ω and the velocity field V coexist and are kinematically related:

$$\Omega = \nabla \times V(r, t) \tag{2}$$

It follows from this relationship that the velocity associated with a straight, finite segment of a vortex line with circulation $\Gamma(t)$ is given by the Biot–Savart law:

$$V(r, t) = \frac{\Gamma(t)}{4\pi} \frac{\omega \times r_1}{\|\omega \times r_2\|_2} [\omega \cdot (\hat{e}_1 - \hat{e}_2)] \tag{3}$$

Here, r is the field point where the velocity is being computed, r_1 and r_2 are the time-dependent position vectors of the field point relative to the ends of the straight vortex segment, \hat{e}_1 and \hat{e}_2 are unit vectors parallel to r_1 and r_2 , and $\omega = r_1 - r_2$. The velocity given by Eq. (3) satisfies Eq. (1) and is irrotational ($\Omega = 0$) everywhere except on the vortex segment.

For a field point on or very near the vortex segment itself or its extension, ω is or nearly is parallel to r_1 . This causes the behavior of $V(r, t)$, as given in Eq. (3), to be troublesome. The troublesome behavior can be easily circumvented by introducing a “cutoff radius” δ into Eq. (3):

$$V(r, t) = \frac{\Gamma(t)}{4\pi} \frac{\omega \times r_1}{\|\omega \times r_2\|_2^2 + (\delta\|\omega\|)^2} [\omega \cdot (\hat{e}_1 - \hat{e}_2)] \tag{4}$$

When the field point approaches the vortex line or its extension, $V(r, t)$, as given in Eq. (4), smoothly becomes the null vector [41]. The influence of the cutoff radius δ on the velocity is strongly felt in the immediate vicinity of the vortex line itself but is hardly noticeable elsewhere. Another option is to use a linear cutoff radius function, in which each vortex element is enclosed by a cylinder and two spherical caps. Within this enclosing region, the velocity decreases linearly toward the vortex line [42].

Standard procedures use a range for the cutoff radius between 10 and 25% of the smallest of the panel dimensions [43].

For a detailed mathematical formulation, the reader can consult the references [44–46].

2. Discretization of the Vortex Sheets

In the UVLM, the bound-vortex sheets (boundary layers) are replaced with a lattice of short, straight vortex segments with constant circulation. These segments divide the surface of the insect’s body and wings into elements of area (panels), which in general are nonplanar, with discrete vortex segments along the edges. The model

is completed by joining free-vortex lines, which represent the free-vortex sheets (wakes), to the bound-vortex lattice along the edges where separation occurs, such as the trailing edges and leading edges of the wings. The locations in which separation occurs are input and are not determined by the solution. However, the vortex lattices representing the wakes (the positions of the vortex segments and the circulations around them) are determined as part of the solution.

Figure 3 shows examples of meshes for the bound-vortex sheets. In both cases, there exists a gap between the wing root and the separation zones (zone 1 for the leading edge and zone 2 for the trailing edge). This adjustment notably improves the shape of the wake near the wing root.

The velocity field associated with the disturbance created by the moving body is the superposition of the fields associated with the vorticity in the bound lattice on the moving body surface and in the freely deforming wakes.

3. Boundary Conditions

The governing equation of the problem is complemented with the following boundary conditions:

1) The regularity at infinity condition requires that the velocity field associated with the disturbance to decay away from the body and its wakes. Hence,

$$\lim_{\|\mathbf{r}\|_2 \rightarrow \infty} \|\mathbf{V}_B(\mathbf{r}, t) + \mathbf{V}_W(\mathbf{r}, t) + \mathbf{V}_{SW}(\mathbf{r}, t)\| = \mathbf{0} \quad (5)$$

where $\|\mathbf{r}\|_2$ is the distance from the body and its wakes, $\mathbf{V}_B(\mathbf{r}, t)$ is the velocity associated with the bound-vortex lattice, $\mathbf{V}_W(\mathbf{r}, t)$ is the velocity associated with the free-vortex lattice being shed from the wing's trailing edge and tip, and $\mathbf{V}_{SW}(\mathbf{r}, t)$ is the velocity associated with the free-vortex lattice being shed from the leading wing's edge. The velocity field obtained from Eq. (4) satisfies this condition.

2) The no-penetration condition requires that, over the entire surface of the insect's body and wings, the normal component of the fluid velocity relative to the body's surface must be zero:

$$(\mathbf{V}_\infty + \mathbf{V}_B + \mathbf{V}_W + \mathbf{V}_{SW} - \mathbf{V}_p) \cdot \hat{\mathbf{n}} = 0 \quad (6)$$

Because the vortex sheets are replaced by vortex lattices, the no-penetration condition given by Eq. (6) is only satisfied at one point in each panel; these are called control points (CPs), and they are located at the centroid of the corners of each panel (see Fig. 3).

In addition to the boundary conditions, there are the following three conditions:

1) There must be continuous pressure in the wake. For an inviscid fluid, the Kelvin–Helmholtz theorem requires that vorticity be

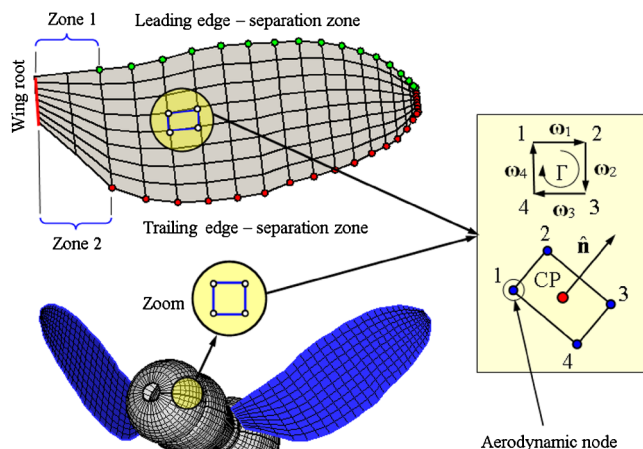


Fig. 3 Discretization of the bound-vortex sheets representing an insect's body and wings.

transported with the fluid particles. This condition is used to obtain the positions of the vortex segments that comprise the lattices representing the wake.

2) There must be spatial conservation of the circulation: the vorticity field is divergenceless. This condition is satisfied by considering the vortex lattices to be composed of closed loops of vortex segments with the same circulation.

3) The unsteady Kutta condition must be satisfied. The pressures on the upper and lower surfaces must vanish along the edges where separation occurs; this requires that all the vorticity generated along these edges be shed, and hence, this condition determines the strength of the vorticity in the wake.

4. Leading-Edge Separation Model

Because the kinematics of winged insects is quite complex, the vortex shedding from the leading edge depends on the angle between the local fluid velocity and the wing plane (effective angle of attack). Several works on leading-edge separation of conventional aircraft wings have reported that flow attached to the wing starts to separate when the angle of attack exceeds a critical value of 12–15 deg [26]. Dickinson and Götz [1] found that at 9 deg (a threshold well below those used by insects) a thin separation bubble, barely visible in the video images, quickly forms on the upper surface of the airfoil and remains stable throughout the duration of translation.

Several authors have developed numerical tools based on vortex-lattice methods that account for leading-edge separation on highly swept delta wings [47–49]. In the present work, we modified and extended an existing UVLM in order to include the effects of leading-edge separation and then used the modified version to calculate the aerodynamic loads on flapping wings. As in the vortex-lattice method, the LEV system is also represented by a family of discrete vortex lines, and the velocity field associated with the leading-edge system is calculated with the Biot–Savart law. This flowfield is added to those generated by the other lattices and the freestream. The leading-edge separation was included by a scheme based upon an on/off mechanism. This mechanism consists mainly of computing the value of the effective angle of attack α_e at each time step and comparing it with a reference value; in the present examples, the reference is $\alpha_c = 12$ deg. If $\alpha_e \geq \alpha_c$, leading-edge separation is included; conversely, if $\alpha_e < \alpha_c$, leading-edge separation is omitted. Once a vortex segment is shed into the wake, it always remains in the wake. In Fig. 4, we present the definition of the angle α_e as well as the wakes shed from both the trailing edge and the leading edge.

5. Aerodynamic Influence Coefficients

Generally, the normal component of the velocity of a fluid particle relative to a control point depends on the superposition of the velocity fields associated with 1) the bound-vortex lattices, 2) the free-vortex lattices, and 3) the freestream. The normal component of the velocity at the control point of i th panel associated with the closed loop of vortex segments with unit circulations along the edges of j th panel is denoted by a_{ij} . Consequently, the normal component of velocity at the control point i associated with all the bound vortices is given by $\sum_{j=1}^N a_{ij}\Gamma_j$, where N is the number of panels in the bound lattices and Γ_j is the magnitude of the circulation around the closed loop of vortex segments along the edges of panel j . The no-penetration condition for the i th panel can be written as follows:

$$\sum_{j=1}^N a_{ij}\Gamma_j + (\mathbf{V}_\infty + \mathbf{V}_W + \mathbf{V}_{SW} - \mathbf{V}_p) \cdot \hat{\mathbf{n}} = 0 \quad (7)$$

where $(\mathbf{V}_p)_i$ is the velocity of body's surface and $\hat{\mathbf{n}}_i$ is the unit vector normal to the surface at the control point of the i th panel. Equation (7) must be simultaneously satisfied at the control points of all the panels, i.e., for $i = 1, \dots, N$. The velocity fields associated with the vorticity in the wakes, the freestream velocity, and the velocity due to the kinematics of the body are already known and can be transferred to the right-hand side (RHS):

$$\text{RHS}_i = -(\mathbf{V}_\infty + \mathbf{V}_W + \mathbf{V}_{SW} - \mathbf{V}_p) \cdot \hat{\mathbf{n}}_i \quad (8)$$

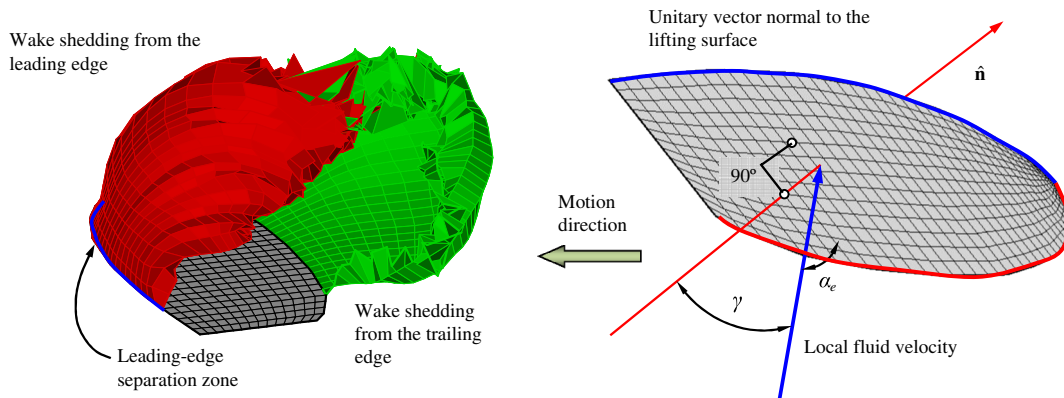


Fig. 4 Separation zones and definition of the angle α_e .

Then, writing Eq. (7) for each panel on the bound-vortex lattice, we obtain the following system of linear equations:

$$\mathbf{A}(t)\mathbf{\Gamma}(t) \equiv \begin{bmatrix} a_{11} & a_{12} & \dots & a_{1N} \\ a_{21} & a_{22} & \dots & a_{2N} \\ \vdots & \vdots & \ddots & \vdots \\ a_{N1} & a_{N2} & \dots & a_{NN} \end{bmatrix} \begin{Bmatrix} \Gamma_1 \\ \Gamma_2 \\ \vdots \\ \Gamma_N \end{Bmatrix} = \begin{Bmatrix} \text{RHS}_1 \\ \text{RHS}_2 \\ \vdots \\ \text{RHS}_N \end{Bmatrix} \quad (9)$$

If the different parts of the insect (head, thorax, abdomen, and wings) are not moving relative to each other, then the influence coefficients are evaluated only once; otherwise, they are reevaluated at each time step. In this work, the head, thorax, and abdomen are modeled as a single rigid body, and the wings have a prescribed motion throughout the entire stroke cycle. Hence, the only parts of the aerodynamic influence matrix $A(t)$, to be updated at each step time are those that take into account the body–wing and the wing–wing aerodynamic interference. Once Eq. (9) is solved, the next step is to calculate the aerodynamic loads.

6. Aerodynamic Loads

The aerodynamic loads on the lifting surfaces (insect's wings) are computed as follows:

1) For each element the pressure jump at the control point is computed with the unsteady Bernoulli equation,

$$\frac{\partial}{\partial t}\Psi(\mathbf{r}, t) + \frac{1}{2}\mathbf{V}(\mathbf{r}, t) \cdot \mathbf{V}(\mathbf{r}, t) + \frac{p(\mathbf{r}, t)}{\rho} = \frac{1}{2}\mathbf{V}_\infty \cdot \mathbf{V}_\infty + \frac{p_\infty}{\rho} \quad (10)$$

where $\partial/\partial t$ denotes the partial time derivative at a fixed location in an inertial reference frame.

2) The force on each element is computed as the product of the pressure jump times the element area obtained from the sum of one-half of the cross products of two vectors along adjoining edges of the panel times the normal unit vector obtained from the cross product of the two diagonals.

3) The resultant forces and moments are computed as the vector sum of the forces and their moments about a common point.

However, as the UVLM is based on thin airfoil theory, it does not account for the leading-edge suction [50], and only the component normal to the noncirculatory velocity is retained, i.e., the contribution of pressure to the local lift. The contribution of the forces on the elements of the lattice to the induced drag/thrust is aligned with the instantaneous noncirculatory velocity, and it can be computed, for example, through the approximation proposed by Katz and Plotkin [26], by the analogy adopted from Sane [35] or by the method developed by Ehlers and Manro [51], in which the leading-edge suction is calculated in the same computer code that evaluates the pressure distribution due to the LEV.

To accurately compute the thrust generated by the flapping motion of a planar wing, the contribution of the leading-edge suction force must be included in the calculations, causing the resultant aerodynamic force vector to tilt toward the leading edge. The calculation of

this force has not been included in the present paper, leading to an underestimation of the total thrust.

In its present form, the evaluation of $\frac{\partial}{\partial t}\Psi(\mathbf{r}, t)$ is problematic, but this term can be put in a form that makes its evaluation relatively easy. Detailed explanations of the treatment of each term in Eq. (10) are given in [44–46].

Once the loads have been computed, the panels in the wakes are “convected” to their new positions by [52]:

$$\mathbf{R}_{\text{node}}(t + \Delta t) \approx \mathbf{R}_{\text{node}}(t) + \mathbf{V}_{\text{node}}(t)\Delta t \quad (11)$$

where Δt is the time increment.

Because all these quantities are functions of time, the question of which instantaneous quantities to use in the approximation is raised. There are several options; for example, one can use the quantities that were calculated at the previous time step, the present time step, or their averaged values for the two time steps. In all cases except the first, iterations are needed, which increase the computational time. Kandil et al. [52] showed that the first option is stable, and there are little differences in the computed results for the various options; therefore, the first option was used to compute all the results in this work.

Then the preceding steps are repeated to find the loads at the next time step.

III. Numerical Results

In this section, we present some results obtained with the present numerical tool relevant to flapping-wing vehicles. The code was written in FORTRAN 90 and compiled to run in Windows platforms. Automatic optimization options, which are specific for Intel processors, have been used to achieve higher performance. For all cases, the code was run on a desktop computer with an i7 processor, RAM DDR3 of 4 GB, and a hard disk of 2 TB.

The results obtained with the present numerical tool were compared with some previously obtained numerical results and experimental data to assess the validity and limitations of the present code. First, we compared the present results for a flapping/twisting wing with the Euler computations of Neef and Hummel [38] and the results obtained by Stanford and Beran [28] using their version of the UVLM. Then, we used force data from robofly experiments published by Dickinson et al. [7]. Finally, we present numerical results for a *Drosophila* in hovering flight.

A. Validation of the Numerical Model

Neef and Hummel considered a rectangular wing with an aspect ratio $AR = 8$, a NACA 0012 airfoil profile, a flapping amplitude of 15 deg, and a reduced frequency of $k = 0.1$ ($k = \omega c/2/V_\infty$, where ω is the flapping frequency and c is the wing chord). The flapping motion is sinusoidal, and an out-of-phase wing rotation (twist) about the leading edge is imposed linearly along the span, with 4 deg of twist at the tip. The flapping period T_f was discretized into 40 equal time steps. Figure 5a provides the kinematic pattern, two sets of

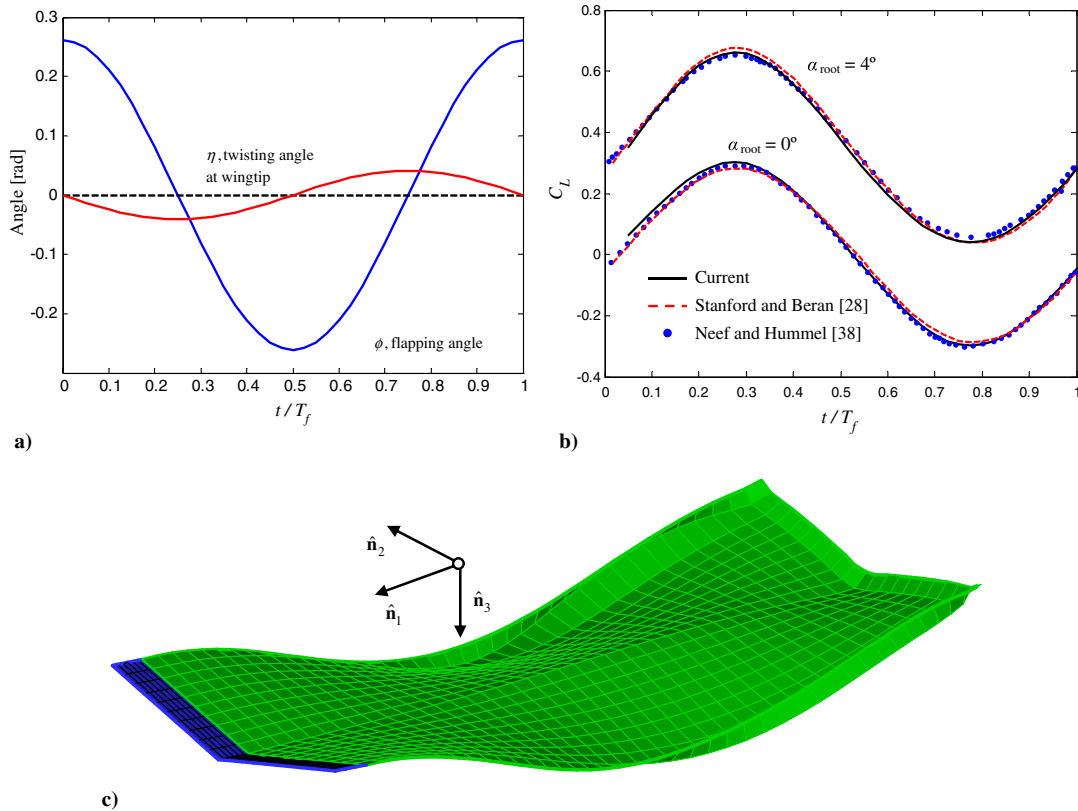


Fig. 5 a) Flapping and twisting motions used by Neef and Hummel [38], b) comparison of the current lift coefficient with results from [28] and [38], and c) a snapshot of the wake evolution (angle of attack of 4 deg).

comparative results of the lift coefficient for a flapping/twisting wing with its root chord inclined at two constant angles of attack of 0 and 4 deg in Fig. 5b, and a snapshot of the wake pattern obtained with the present aerodynamic model in Fig. 5c. In Fig. 5b, the agreement among the three sets of results is excellent. The slight discrepancies between the lift force computed by Stanford and Beran [28] and the lift force calculated in this work can be attributed to the specification of some user-defined parameters, such as the cutoff radius and differences in the two versions of Bernoulli's equation. It is evident in Fig. 5c that the wing-tip vortex system has been omitted. The wing has a fairly large aspect ratio, and it is likely that this does not affect the loads much. The wing-tip-vortex system was also ignored by Stanford and Beran [28].

B. Force Comparison with Robofly Experiments

Using the present aerodynamic model, we obtained the lift forces from numerical simulations and compared them with the experimental data reported by Dickinson et al. [7]. The experiment they carried out consists of a dynamically scaled model of a *Drosophila Melanogaster*, dubbed robofly. The motion of the two wings was driven by an assembly of six computer-controlled stepper motors, and each wing was capable of rotational motion about three axes. The wings were immersed in a 1×2 m cross-section tank filled with mineral oil ($\rho_{oil} = 880 \text{ kg/m}^3$, $\nu_{oil} = 115 \text{ cSt}$). Robofly's wings have a length of 25 cm (from the force sensor to the wing tip), are made of Plexiglas®, and were cut according to the planform of a *Drosophila* wing. The wing executed an insectlike flapping motion at a frequency of 0.145 Hz with the wing tip tracing out a flattened figure of eight. The viscosity of the oil, the length of the wing, and the flapping frequency were chosen in order to match the Reynolds number Re typical of the flight of a fruit fly ($Re = 136$). The kinematic pattern employed by Dickinson's team consists of a stroke amplitude of 160 deg, and an angle of attack at midstroke of 40 deg for both upstroke and downstroke. Three different phase relations between the wing rotation and the reversal stroke were used:

- 1) The wing rotation precedes the reversal stroke by 8% of the wing-beat cycle.
- 2) The wing rotation occurs symmetrically with respect to the reversal stroke.
- 3) The wing rotation is delayed with respect to the stroke reversal by 8% of the stroke cycle.

Figure 6 shows the robofly mechanism, the wing planform of the robofly, and the kinematic patterns used by Dickinson et al. [7].

Three numerical simulations were obtained to determine the effect of the different phase relations between wing rotation and reversal stroke. The wing-beat cycle was discretized in 100 time steps, and each wing was discretized into 384 aerodynamic panels. We use two different values for the cutoff radius. We use a cutoff radius $\delta = 0.15$ (15%) to compute the influence of the trailing-edge vortex over itself and over the bounded sheet. For computing the LEV influence over itself and over the bounded sheet, we use a cutoff radius $\delta = 0.20$ (20%). Cutoff radius values smaller than 20% for LEV produce too much noise on lift forces. It is noteworthy that the ad hoc procedure used in this paper uses an embedded cutoff. Furthermore, the modified singular core $\mathbf{K}(\mathbf{R} - \mathbf{R}_0; \delta)$ in Eq. (4) depends on the magnitude of vorticity segment. This feature makes this technique well suited to treat problems involving structures undergoing complex motions.

In Fig. 7, we present numerical results for the lift force with and without considering leading-edge separation and compare them with those obtained in Dickinson's experiment described earlier.

The results from the aerodynamic model that includes leading-edge separation are in remarkable agreement with the experimental data. On the other hand, the lift curve obtained with and without leading-edge separation coincides almost exactly in the rotational phases (reversal stroke). Some differences can be appreciated on the translational phases (downstroke/upstroke), in which previous studies have shown that the LEV is particularly important and contributes substantially to the lift forces. Quantitatively, the maximum difference is 19% and occurs basically in the second half-stroke. The pair of opposite spikes at stroke reversals is well captured

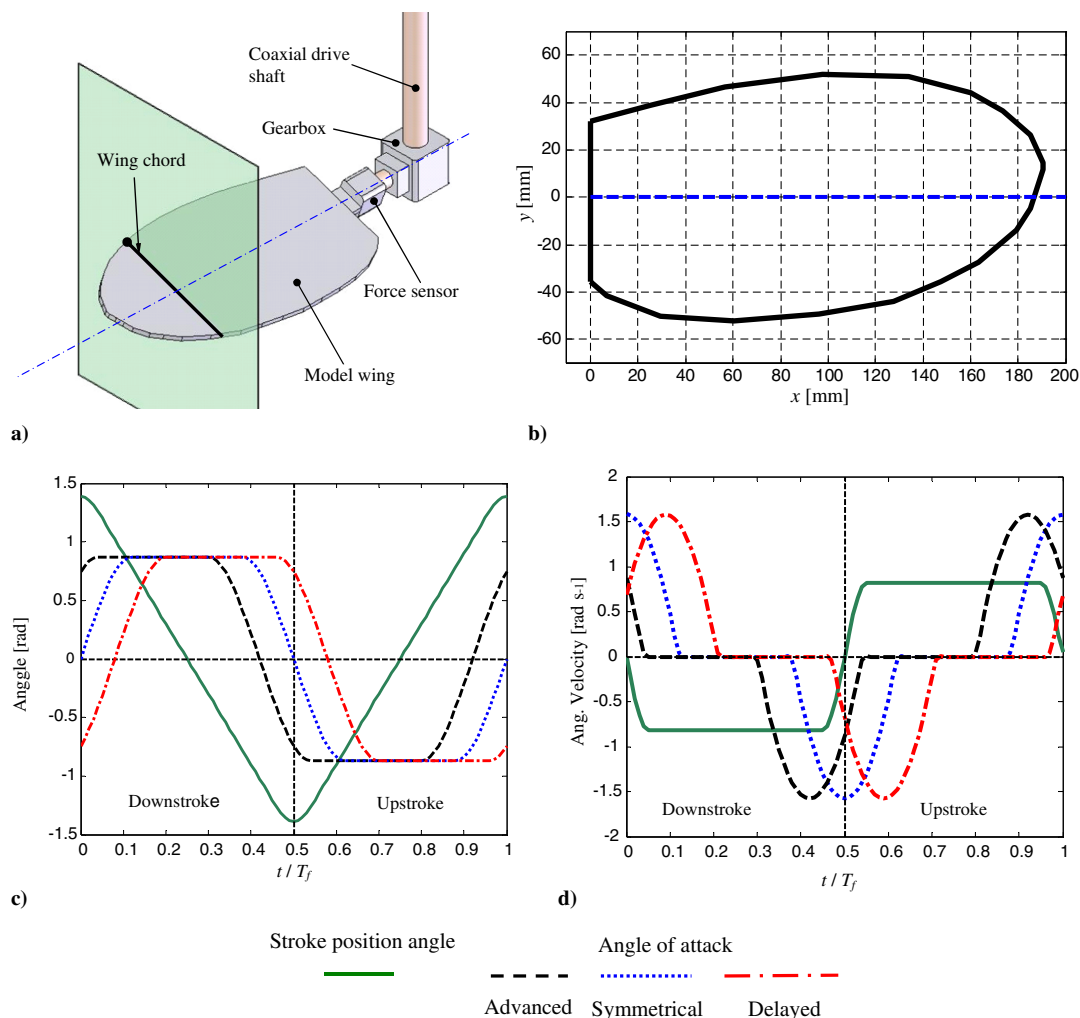


Fig. 6 a) Robofly apparatus (reproduction of Dickinson et al. [7]), b) wing planform of the robofly used for numerical simulations, c) stroke position angle and angle of rotation of the wing for three different rotational timings, and d) time derivative of the stroke position angle and time derivative of the rotation angle for three rotational timings.

by the numerical model. They occur at the same points in time without any significant lag, thus accounting well for unsteadiness of the flow. Moreover, the magnitudes of the negative and positive spikes for lift are consistent with the experimental data.

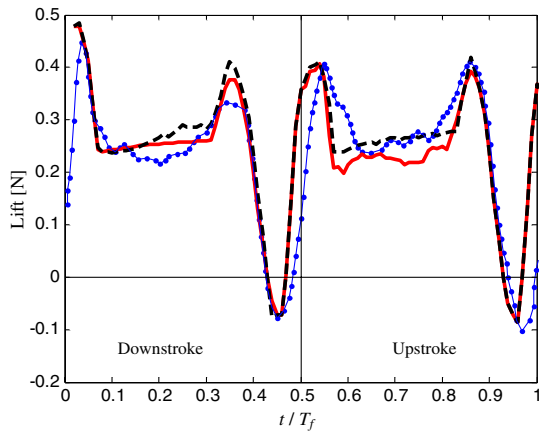
The results presented here are very encouraging because they show better agreement than those in previously published comparisons, as for instance the CFD study by Sun and Tang [13], which showed relatively poor agreement with the experiments of Dickinson et al. [7], and the 2-D UVLM model combined with the blade-element theory developed by Ansari et al. [8,9], which showed similar trends for lift and thrust forces, but the magnitudes of the positive and negative spikes for lift and thrust overestimated the experimental measures reported by Birch and Dickinson [53].

There is much evidence that flying insects actively change their wing kinematics in order to optimize the aerodynamic forces throughout a specific maneuver. In fact, the forces produced by insects are very sensitive to the rotational timing, which is consistent with the kinematic changes exhibited by *Drosophila* during steering behaviors. According to these results, by advancing the timing of rotation on both wings, a fly could generate the symmetrical increase required for forward or upward acceleration. As shown in Fig. 7, the trend and magnitude of lift associated with the three cases analyzed in the preceding paragraphs (advanced, symmetrical, and delayed patterns) have been successfully captured by the current model. These results are significant because they justify the use of the UVLM to study the 3-D aerodynamic behavior of insects executing different maneuvers. Figure 8 shows the temporal evolution of the wake of the robofly for the case of advanced pattern.

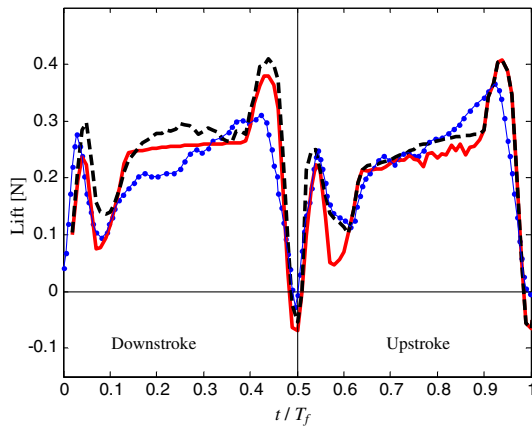
Another remarkable feature shown in Fig. 7 is the synchrony between the experimental measurements and the numerical predictions obtained from the current vortex-lattice model. To properly appreciate this feature, we compute the discrete fast Fourier transform for the force data from numerical simulations and experiments. This analysis is presented in Fig. 9 only for the lift force shown in Fig. 7a (advanced pattern); a similar analysis can be carried out for symmetrical and delayed patterns.

The frequency content for Dickinson's data clearly shows the flapping frequency of the motion (point A in Fig. 9, $n_f = 0.1446$ Hz) and twice this frequency (point B in Fig. 9, $2n_f = 0.2893$ Hz) together with a number of harmonics. These harmonics appear because there are two half-strokes per wing-beat cycle (the wing-passing frequency). Moreover, the frequency content of the lift force computed by the current model closely matches the flapping frequency of the motion ($n_f = 0.145$ Hz and $2n_f = 0.29$ Hz). Another estimate of the quality of the numerical model can be inferred by comparing the values of the mean lift \bar{L} . The square and circular symbols in Fig. 9 represent the experimental mean lift force (0.2301 N) and the computed mean lift force (0.2406 N), respectively. The difference between the experimental and numerical mean lift force is barely of 4.5%.

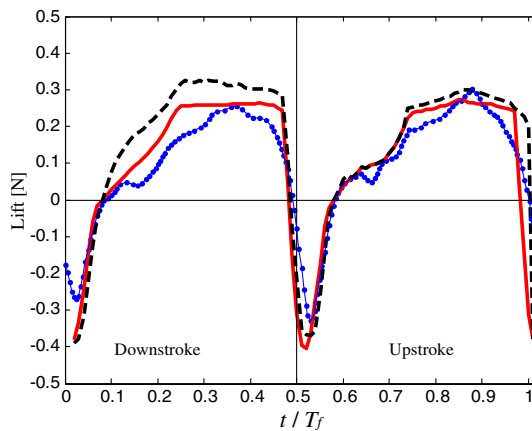
It is noteworthy that the reference value α_c at which vorticity shedding from the leading edge begins does not have a significant influence on the results presented in the preceding paragraphs. Specifically, we investigated a range between 8 and 15 deg for α_c , noticing slight differences that do not affect the shape and magnitude of the lift force. This analysis was performed for each of the motion patterns considered.



a)



b)

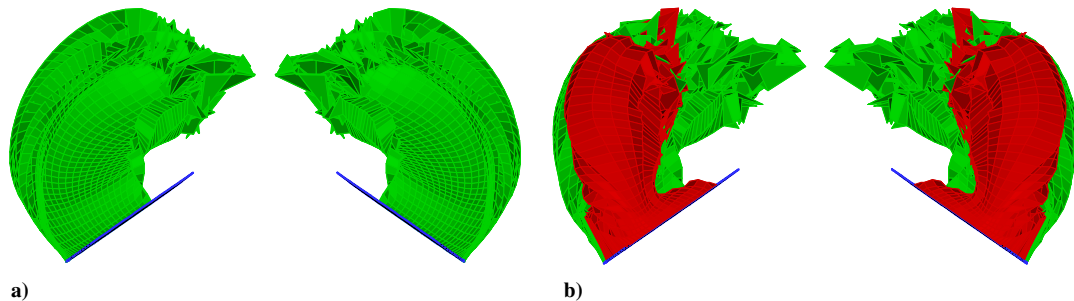


c)

With LEV Without LEV Dickinson et al. [7]

--- — —●—

Fig. 7 Comparison of numerical results and experimental measurements for the robofly apparatus (first stroke cycle): a) advanced pattern, b) symmetrical pattern, c) delayed pattern.



a)

b)

Fig. 8 Robofofly wake pattern: a) without LEV and b) with LEV.

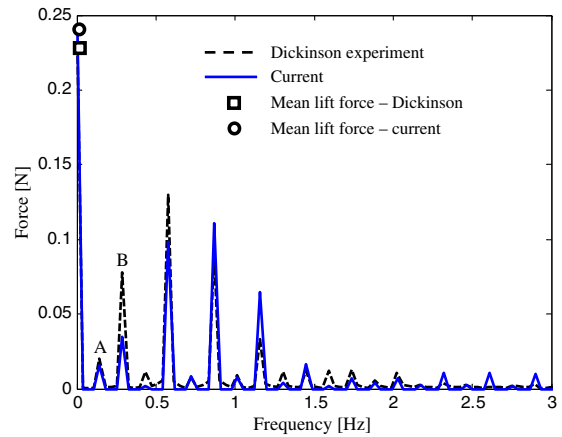


Fig. 9 Comparison of frequency content of robofly force data from Dickinson et al. [7] with results from the current numerical simulation (advanced pattern).

The fact that the frequency content and the mean lift force between the experimental and numerical data are so similar implies that the underlying physical phenomena (e.g., vortex shedding) are well captured. The extended UVLM model developed and implemented in this work is based on an asymptotic approximation to the solution of the Navier–Stokes equations that improves as the Reynolds number increases; it has, at times, been referred to as the infinite-Reynolds-number approximation. This model recognizes viscous effects as being responsible for the presence of a boundary layer on the surface of the body, but the analysis of the viscous flow in the boundary layer is not included (flow separation, transition, and reattachment, among other phenomena [54]). Therefore, with this approximation, the locations of separation from the body’s surface cannot be predicted but must be input, such as at the leading edge, wing tip, etc. Outside the boundary layer, the flow is governed by the incompressible version of Euler’s equation (Laplace’s equation). Only the pressure on the surface of the body, as predicted by this inviscid outer flow, is used to determine the forces; thus, the predicted loads are due solely to inertial effects. These calculated loads are, for the cases considered here, in extraordinarily good agreement with experimental results in tendency, synchronism, and magnitude. Because viscous effects were not included for the cases considered here, it seems reasonable to interpret the present results as an indication that inertial effects dominate viscous effects, at least for some flights at small scales. Moreover, the results, for the cases presented here, definitely show the interaction among vortices to be the main feature, which allows insects to generate enough lift to stay aloft. This finding suggests the strong likelihood that the UVLM could be a very accurate and efficient tool for future studies of insect aerodynamics.

The wing mesh and time-step size used to carry on the numerical simulations presented in the preceding paragraphs were determined by means of a simplified study of the influence of the panel density on the lift. Such a convergence analysis was performed for the advanced motion pattern; similar results were obtained for the other two motion patterns (symmetrical and delayed). These results are presented in Table 2.

Table 2 Convergence analysis

Case/density mesh	$\Delta t/T_f$	Step time	Mean lift, N	Frequency, Hz
Experimental	—	—	0.23010	0.1446–0.2893
Numerical				
12 panels	0.040	25	0.27159 (+18.0%)	0.145–0.290
72 panels	0.020	50	0.27684 (+20.0%)	0.145–0.290
120 panels	0.020	50	0.24359 (+5.8%)	0.145–0.290
384 panels	0.010	100	0.24060 (+4.5%)	0.145–0.290
1200 panels	0.005	200	0.23352 (+1.5%)	0.145–0.290

In Fig. 10, we show the lift force for each case study reported in Table 2; solid line with circular markers for 12 panels, dotted line for 72 panels, center line for 120 panels, solid line for 384 panels and broken line for 1200 panels per wing. The analysis of the five cases presented in Table 2 shows that for a poor discretization (12 or 72 panels per wing) the lift force exhibits significant variations, which is also reflected in a mean lift value much larger than the value reported by Dickinson et al. [7]. As the mesh is refined lift curves show no significant variations (Fig. 10a) and the mean lift approaches the experimental results (Fig. 10b). Furthermore, the frequency contents of the lifts are essentially the same. This characteristic is because the general form of these curves is properly captured, even for poor aerodynamic meshes. However, it should be noted that the high-density mesh (1200 panels) shows a marked difference immediately after supination (approximately 18%). In this case, one can see, moreover, a slight interference in the upstroke, which is possibly due to an excessive refinement of the mesh [44,52,55]. It is also noteworthy that the computational cost grows enormously as the mesh is refined. A typical run for a mesh composed by 384 panels takes approximately 55 min, whereas the run time is increased to 5 h

for a mesh composed by 1200 panels. In summary, we conclude that aerodynamic meshes discretized with 120 and 384 panels produce very good results.

C. Numerical Simulations of the Aerodynamics of a Fruit Fly in Hover

As a test of the versatility of the present numerical tool, numerical results for the aerodynamics of a fruit fly in hover are presented. Data reported by Fry et al. [56] and Bos et al. [57] on the actual kinematics of a fruit fly in hover were used to describe the wing motion over a flapping cycle (see Fig. 11a); solid line for the stroke deviation angle, dotted line for the stroke position angle and broken line for the rotation angle. This model was derived from measurements on real fruit flies and is therefore considered to be the most realistic representation of fruit-fly kinematics. The adopted kinematics includes the deviation angle, which results in a figure-of-eight pattern (see Fig. 11b).

To obtain the curves presented in Fig. 11a we performed a least-squares fit using Fourier series over a set of discrete values coming from experimental measurements (circular markers). In Fig. 11b, we

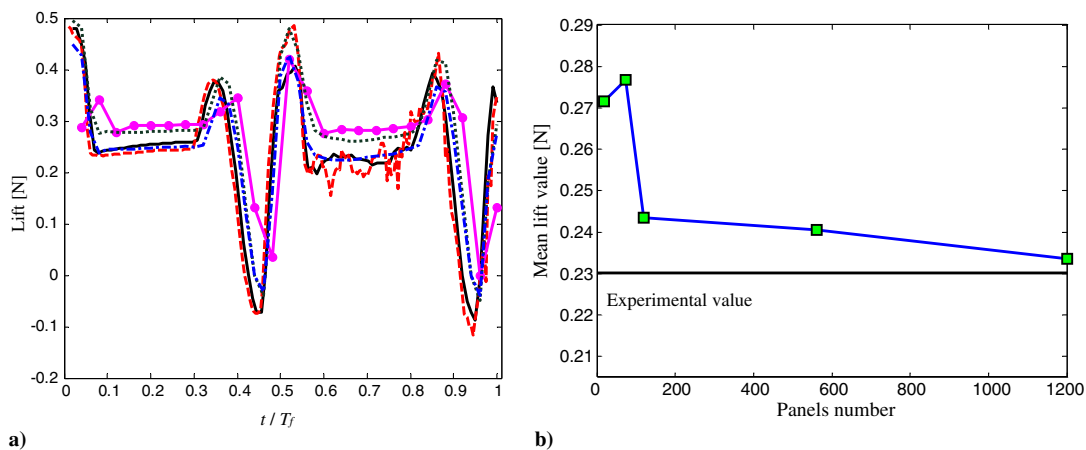


Fig. 10 a) Lift force for the advanced pattern motion (first cycle) and b) mean lift value vs panels number.

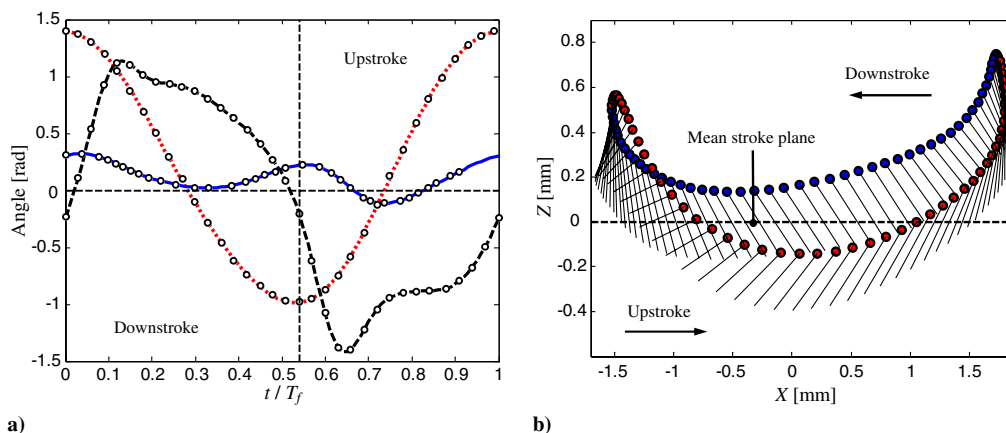


Fig. 11 a) Actual kinematics of a fruit fly in hovering; circular markers indicate experimental data. b) Trajectory of the wing-tip (figure of eight).

present a numerical simulation of the wing-tip path of a fruit fly in hover. For a better visualization, the wing-tip trajectory was projected onto the sagittal plane [40,58], and small circles mark the leading edge. The line attached to these points at each instant represents a portion of the wing's chord and indicates the orientation of the wing's cross section during the flapping cycle.

The setup of the numerical experiment shown in this section consists of 1) a flapping frequency $n_f = 220$ Hz, 2) a wing length $R = 2.5$ mm and wing area $S = 2.21$ mm², and 3) a fully spatial discretization of the insect with 3448 aerodynamic panels and 100 step times. These magnitudes correspond to a Reynolds number of

133 for a 3-D flapping wing in hover ($Re_{3D} = 4\Phi n_f R^2 / (v_{air} AR)$, where Φ is measured in radians) [34,56]. Because of the complex motion that the wings experience during a stroke cycle as product of a real kinematics (a slightly deformed eight pattern), the wake shed from the leading edge during the downstroke is cut by the wing when it moves in the opposite direction (upstroke). Because this issue was not addressed in the present framework, the LEV is excluded in this analysis. Figure 12 shows the wake pattern for the first half-stroke.

Figure 12 shows how the fluid particles are driven down as they are shed from the sharp edges, thereby revealing the presence of lift. In addition, it can be seen that the aerodynamic model used in this work

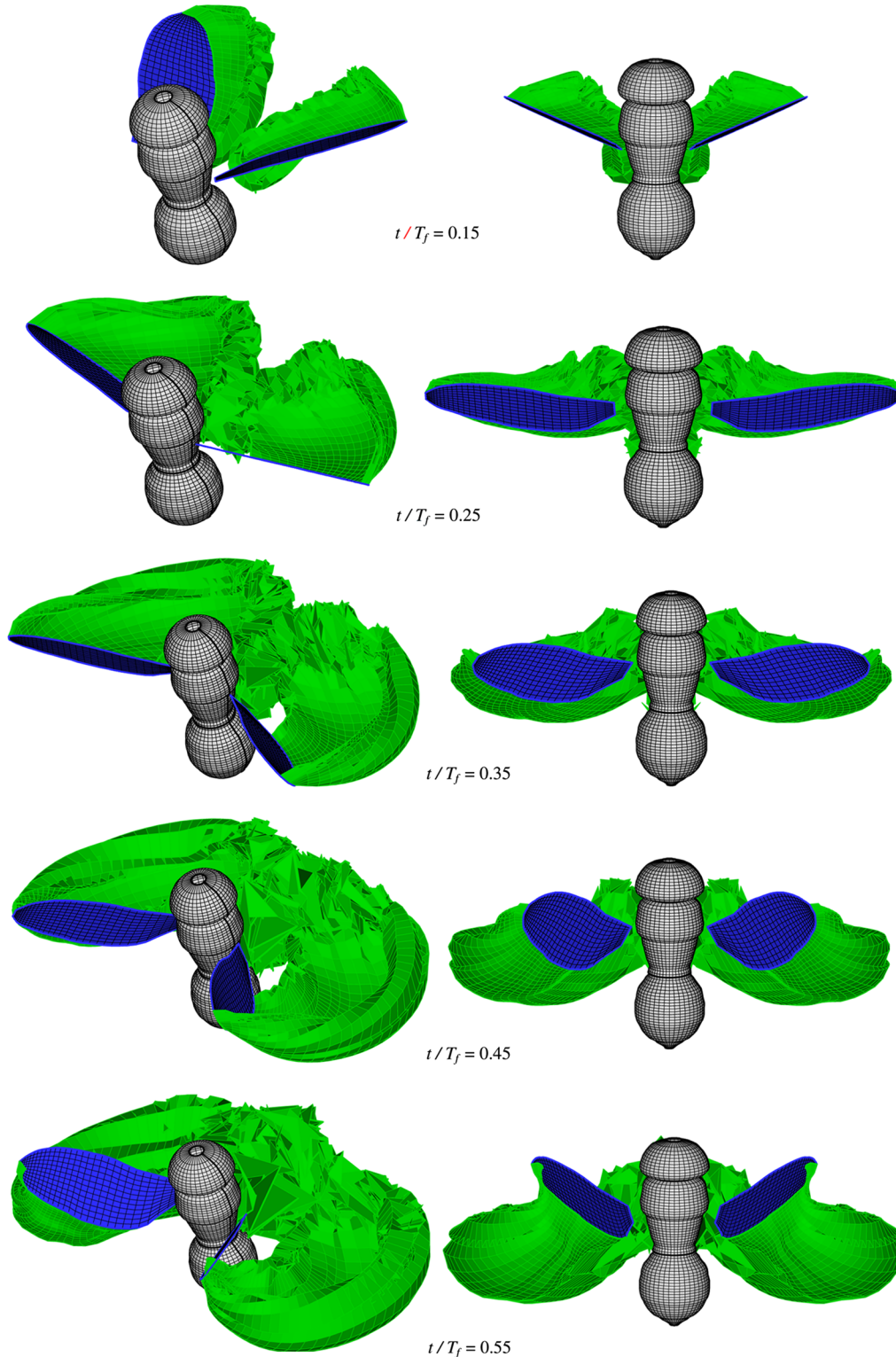
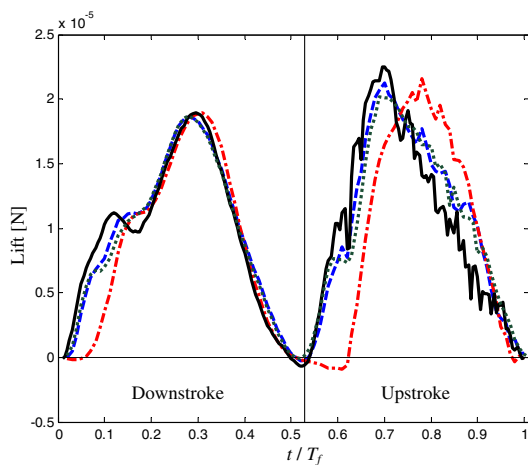


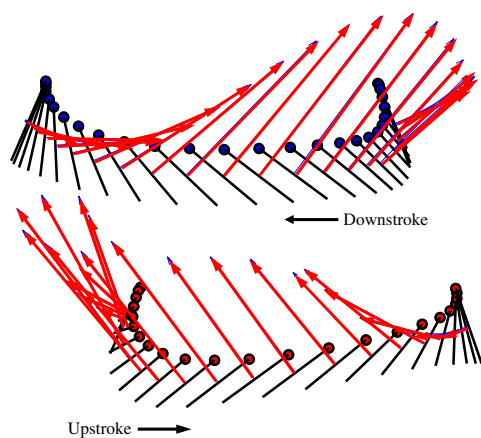
Fig. 12 Wake pattern for the first half-stroke.

captures in great detail the simultaneous aerodynamic interference among the insect's body and wakes, the insect's wings and wakes, and the two wakes.

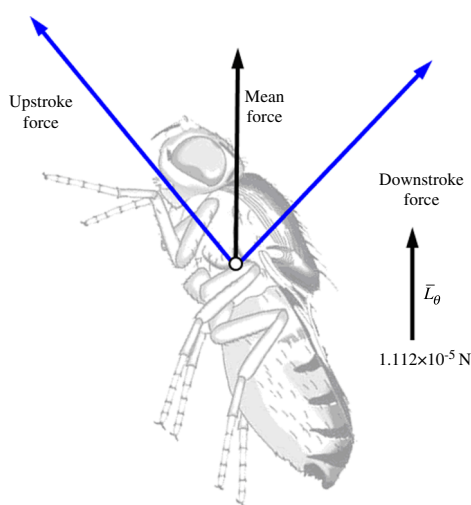
Figure 13 shows the lift force for a full stroke cycle and the diagram of the wing motion indicating the magnitude and orientation of the instantaneous force vectors generated throughout the stroke cycle (broken line for lift considering deviation angle and the insect's body; center line for lift with a null deviation angle considering the



a)



b)



c)

Fig. 13 a) Lift force for the first stroke cycle (real kinematics of a *Drosophila* in hover) b) instantaneous force vectors superimposed on a diagram of wing motion for the real kinematics presented in Fig. 11a and c) force balance during hovering; the mean flight force is computed from the data plotted in Fig. 13a.

insect's body; solid line for lift considering deviation angle, the insect's body and a time-step halved; and dotted line for lift considering deviation angle and without insect's body). In Fig. 13b, black lines indicate the position of the wing at several temporally equidistant points during each half-stroke. Small circles mark the leading edge.

The effect of the realistic fruit fly's wing kinematics results in forces that differ significantly from those obtained from simplified wing kinematic models commonly used in the literature. The most obvious particularity of the realistic fruit-fly model is the extra "bump" in the angle of attack just after the stroke reversal, compared to the robofly model (see Fig. 11a). From Fig. 13b, it is observed that the extra bump generates an increase in lift at the beginning of both downstroke and upstroke. After the bump the angle of attack more or less matches the plateau found in robofly, which results in an almost constant force distribution (see Fig. 13b).

Another important issue present in the realistic fruit-fly model is the deviation from the stroke plane. This deviation causes a figure of eight instead of a flat pattern. Because deviation may introduce a large velocity component perpendicular to the stroke plane, the effective angle of attack is increased just after each reversal stroke. On the contrary, at the end of a stroke the wing moves up again, which leads to a decrease in the effective angle of attack. The complex features associated with the deviation are reflected on the aerodynamic forces by a severe reduction in the lift at the end of each stroke (where the vector forces have almost a horizontal direction) and a subsequent increase of it just after each rotational phase. In summary, the deviation is leveling the force distributions, whereas the mean lift remains practically unaffected. We tested this peculiarity by performing numerical simulations with and without deviation and found that the mean lift force considering deviation is 12% higher than a configuration with a null deviation angle ($\bar{L}_\theta = 1.112 \times 10^{-5}$ N and $\bar{L}_{\theta=0} = 0.9881 \times 10^{-5}$ N, where the subscripts θ and $\theta = 0$ indicate with and without deviation, respectively). This leads to the suggestion that a *Drosophila* could be using this deviation to level the wing loading and as a possible instrument of control to stabilize the flight when the creature is executing different maneuvers.

The results presented in this section were computed only for the first stroke cycle, and therefore, these contain initial transients. To assess the time convergence of these results, we performed a numerical simulation with a time-step halved, obtaining a lift curve with a little noise in the second translational phase (upstroke) (see solid line in Fig. 13a). It is because a time-step halved implies a refinement of the aerodynamic mesh, and therefore, the wake becomes messy from the second translational phase onward. With respect to the insect's body presence, it does not affect the lift force for the flight configuration studied in this work (dotted line in Fig. 13a). Certainly, this flight configuration, a hover mode, is symmetrical, and therefore, we cannot make general conclusions about the influence of the insect's body on the aerodynamic forces. A complete study of this nature should involve nonsymmetrical flight conditions and inclined air streams.

Finally, we investigated whether the insect's weight can be balanced by the mean force \bar{L}_θ calculated from the lifting force considering deviation angle presented in Fig. 13a. Data for the weight of a *Drosophila Melanogaster* were taken from Fry et al. [59]. They used a technique based on a measured relationship between the wing's length and the body's mass (sample number $N = 53$) to estimate the mass of a fly and found that it lies between 1.16 and 1.40 mg, which corresponds to a weight in the range of 11.4 to 13.7 μ N. For the simulation shown in this section, the average vertical force throughout the stroke was 11.12 μ N, which, in principle, is sufficient to support the weight of a fruit fly. Moreover, it must be emphasized that in this case the leading-edge separation was not taken into account, an effect that undoubtedly increases the lift forces during the translational phases as stated in Sec. III.B.

D. Limitations of the Model

Although the numerical results obtained with the present model have quite accurately matched experimental observations (Fig. 7) and

have been able to predict good results for an insect in hover (Figs. 12 and 13), it still is an inviscid model and, therefore, has some limitations.

One such limitation is that the present aerodynamic model is the result of an asymptotic approximation to the Navier–Stokes equations for a Reynolds number tending to infinity that does not include an analysis of the boundary layer, and therefore, viscous effects are not captured by the model. The only effect incorporated into the current model is the phenomenon of leading-edge separation by means of a simple scheme based upon an on/off mechanism (Sec. II.C.4).

Sometimes, in the computation of the velocity from the Biot–Savart law, a control point happens to be very close to a vortex segment. The result is an unreasonably high predicted velocity and therefore an excessive displacement of the aerodynamic nodes (connectors) defining each vortex segment in the wake. These numerical instabilities are much more significant in flight configurations in which the wakes remain close around the insect's body and wings, hovering being an extreme condition (in which the freestream velocity is zero). Another significant limitation is related to the common situation when a hovering wing cuts through its own wake; this issue is not addressed in this work, but definitely it should be considered in future work.

Future research should include the investigation of a mechanism to combine the UVLM with the vortex-particle method in order to improve the spatial description of the wakes, run several stroke cycles, and improve the performance of the model in multiple flight configurations [30,60,61]. In addition, the use of the fast multipole tree to rapidly compute the velocity contribution from the time-varying wakes should be explored [30,60–62].

Despite the limitations outlined in the preceding paragraphs, the modified model presented in this article is an excellent tool for studying the aerodynamics of flying insects and small birds.

IV. Conclusions

In this paper, the development of a computational tool that is an extension of the three-dimensional version of the unsteady vortex-lattice method (UVLM) was described. The aerodynamic model was properly modified to include leading-edge separation. To consider insects with dissimilar morphologies and several sizes, a preprocessor was developed that allows one to 1) generate diverse geometries for the insect's body (head, thorax, and abdomen) and wings and 2) use different kinematic patterns for the motion of the wings.

Some important conclusions can be drawn from the results presented in the preceding sections. These results help to better understand the underlying physics associated with the aerodynamics of flapping wings whose complexity is well accepted but at the same time usually not well understood.

The model was validated by comparing its results with Dickinson's experimental data. The lift force predicted by the current model showed extraordinarily good agreement in trend and magnitude with the experimental data obtained from the robofly for three different timings between the wing's rotation and reversal stroke. Comparison of frequency contents of this time-dependent flow highlighted the temporal consistency between the model results and the experimental data. Finally, it was found that the average vertical force computed with the fruit-fly model in hovering is sufficient to bear its weight throughout the stroke cycle.

These results show that the present aerodynamic model is indeed capable of predicting, with notable accuracy, the forces and the flowfield generated by insectlike flapping wings. The similarity found in tendency, synchronism, and magnitude among the lift forces when compared against experimental results shows that the underlying flow features are also well captured. Moreover, it seems reasonable to interpret the present results as an indication that inertial effects dominate viscous effects, at least for some flights at small scales, and show the interaction among vortices to be the main feature, which allows insects to generate enough lift to stay aloft. This finding suggests the strong likelihood that the UVLM could be a very accurate and efficient tool for future studies of insect aerodynamics.

Another feature that makes the current strategy attractive is the low computational cost compared to computational fluid dynamics simulations, finite element approaches, or direct numerical simulations.

Although the numerical tool presented here is a good start toward a better understanding of the aerodynamic behavior of insect flight, in the future, it will be necessary to carry out simulations that include structural dynamics, control systems, and highly complex flight conditions in indoor and outdoor environments.

Currently, a numerical algorithm is being developed to combine the aerodynamic model presented in this work with a dynamical model based on a multibody approach also being developed by the authors.

Acknowledgments

This work was partly supported by the Consejo Nacional de Investigaciones Científicas y Técnicas, Argentina. The authors would like to thank the Grupo de Electrónica Aplicada, Engineering School, Universidad Nacional de Río Cuarto, Argentina.

References

- [1] Dickinson, M. H., and Götz, K., "Unsteady Aerodynamic Performance of Model Wings at Low Reynolds Numbers," *Journal of Experimental Biology*, Vol. 174, 1993, pp. 45–64.
- [2] Ellington, C. P., "The Aerodynamics of Hovering Insect Flight: IV. Aerodynamics Mechanisms," *Philosophical Transactions of the Royal Society of London, Series B: Biological Sciences*, Vol. 305, No. 1122, 1984, pp. 79–113.
doi:10.1098/rstb.1984.0052
- [3] Van den Berg, C., and Ellington, C. P., "The Three-Dimensional Leading-Edge Vortex of a 'Hovering' Model Hawkmoth," *Philosophical Transactions of the Royal Society of London, Series B: Biological Sciences*, Vol. 352, No. 1351, 1997, pp. 329–340.
doi:10.1098/rstb.1997.0024
- [4] Ellington, C. P., Van den Berg, C., Willmott, A. P., and Thomas, A. L. R., "Leading-Edge Vortices in Insect Flight," *Nature (London)*, Vol. 384, Dec. 1996, pp. 626–630.
doi:10.1038/384626a0
- [5] Vest, M., and Katz, J., "Unsteady Aerodynamic Model of Flapping Wings," *AIAA Journal*, Vol. 34, No. 7, 1996, pp. 1435–1440.
doi:10.2514/3.13250
- [6] Ramamurti, R., and Sandberg, W. C., "A Three-Dimensional Computational Study of the Aerodynamic Mechanisms of Insect Flight," *Journal of Experimental Biology*, Vol. 205, 2002, pp. 1507–1518.
- [7] Dickinson, M. H., Lehmann, F.-O., and Sane, S. P., "Wing Rotation and the Aerodynamic Basis of Insect Flight," *Science*, Vol. 284, No. 5422, 1999, pp. 1954–1960.
doi:10.1126/science.284.5422.1954
- [8] Ansari, S. A., Żbikowski, R., and Knowles, K., "Non-Linear Unsteady Aerodynamics Model for Insect-Like Flapping Wings in the Hover. Part 1: Methodology and Analysis," *Journal of Aerospace Engineering*, Vol. 220, No. 2, 2006, pp. 61–83.
doi:10.1243/09544100JAERO49
- [9] Ansari, S. A., Żbikowski, R., and Knowles, K., "Non-Linear Unsteady Aerodynamics Model for Insect-Like Flapping Wings in the Hover. Part 2: Implementation and Validation," *Journal of Aerospace Engineering*, Vol. 220, No. 3, 2006, pp. 169–186.
doi:10.1243/09544100JAERO50
- [10] Von Karman, T., and Sears, W. R., "Airfoil Theory for Nonuniform Motion," *Journal of the Aeronautical Sciences*, Vol. 5, No. 10, 1938, pp. 379–390.
- [11] Liu, H., and Kawachi, K., "A Numerical Study of Insect Flight," *Journal of Computational Physics*, Vol. 146, No. 1, 1998, pp. 124–156.
doi:10.1006/jcph.1998.6019
- [12] Liu, H., Ellington, C. P., Kawachi, K., Van den Berg, C., and Willmott, A. P., "A Computational Fluid Dynamics Study of Hawkmoth Hovering," *Journal of Experimental Biology*, Vol. 201, 1998, pp. 461–477.
- [13] Sun, M., and Tang, J., "Unsteady Aerodynamic Force Generation by a Model Fruit Fly Wing in Flapping Motion," *Journal of Experimental Biology*, Vol. 205, 2002, pp. 55–70.
- [14] Sun, M., and Tang, J., "Lift and Power Requirements of Hovering Flight in *Drosophila Virilis*," *Journal of Experimental Biology*, Vol. 205, 2002, pp. 2413–2427.

- [15] Dickinson, M. H., "The Effects of Wing Rotation on Unsteady Aerodynamic Performance at Low Reynolds Numbers," *Journal of Experimental Biology*, Vol. 192, 1994, pp. 179–206.
- [16] Sun, M., and Du, G., "Lift and Power Requirements of Hovering Insect Flight," *Acta Mechanica Sinica*, Vol. 19, No. 5, 2003, pp. 458–469.
- [17] Sun, M., and Wu, J. H., "Lift Generation and Power Requirements of Fruit Fly in Forward Flight with Modeled Wing Motion," *Journal of Experimental Biology*, Vol. 206, Sept. 2003, pp. 3065–3083. doi:10.1242/jeb.00517
- [18] Tang, J., Viieru, D., and Shyy, W., "Effects of Reynolds Number, Reduced Frequency and Flapping Kinematics on Hovering Aerodynamics," *45th AIAA Aerospace Sciences Meeting and Exhibit*, Reno, Nevada, AIAA Paper 2007-0129, 2007.
- [19] DeLaurier, J. D., "An Aerodynamic Model for Flapping Wing Flight," *Aeronautical Journal*, Vol. 97, 1993, pp. 125–130.
- [20] Belotserkovskii, S. M., "Study of the Unsteady Aerodynamics of Lifting Surfaces Using the Computer," *Annual Review of Fluid Mechanics*, Vol. 9, Jan. 1977, pp. 469–494. doi:10.1146/annurev.fl.09.010177.002345
- [21] Rehbach, C., "Numerical Calculation of Three Dimensional Unsteady Flows with Vortex Sheets," *AIAA 16th Aerospace Sciences Meeting*, Huntsville, Alabama, AIAA Paper 1978-0111, 1978.
- [22] Atta, E. H., Kandil, O. A., Mook, D. T., and Nayfeh, A. H., "Unsteady Aerodynamic Loads on Arbitrary Wings Including Wing-Tip and Leading-Edge Separation," *AIAA Paper 1977-0156*, 1977.
- [23] Konstantinopoulos, P., Thrasher, D. F., Mook, D. T., Nayfeh, A. H., and Watson, L., "A Vortex-Lattice Method for General Unsteady Aerodynamics," *Journal of Aircraft*, Vol. 22, No. 1, 1985, pp. 43–49. doi:10.2514/3.45078
- [24] Levin, D., and Katz, J., "Vortex-Lattice Method for the Calculation of Nonsteady Separated Flow Over Delta Wings," *Journal of Aircraft*, Vol. 18, No. 12, 1981, pp. 1032–1037. doi:10.2514/3.57596
- [25] Katz, J., "Lateral Aerodynamic of Delta Wings with Leading-Edge Separation," *AIAA Journal*, Vol. 22, No. 3, 1984, pp. 323–328. doi:10.2514/3.8395.
- [26] Katz, J., and Plotkin, A., *Low-Speed Aerodynamics*, 2nd ed., Cambridge Univ. Press, New York, 2001, pp. 421–495.
- [27] Fritz, T. E., and Long, L. N., "Object-Oriented Unsteady Vortex Lattice Method for Flapping Flight," *Journal of Aircraft*, Vol. 41, No. 6, 2004, pp. 1275–1290.
- [28] Stanford, B. K., and Beran, P. S., "Analytical Sensitivity Analysis of an Unsteady Vortex-Lattice Method for Flapping-Wing Optimization," *Journal of Aircraft*, Vol. 47, No. 2, 2010, pp. 647–662. doi:10.2514/1.46259
- [29] Ghommem, M., Hajj, M. R., Mook, D. T., Stanford, B. K., Beran, P. S., Snyder, R. D., and Watson, L. T., "Global Optimization of Actively Morphing Flapping Wings," *Journal of Fluids and Structures*, Vol. 33, Aug. 2012, pp. 210–228. doi:10.1016/j.jfluidstructs.2012.04.013
- [30] Willis, D. J., Peraire, J., and White, J. K., "A Combined pFFT-Multipole Tree Code, Unsteady Panel Method with Vortex Particle Wakes," *International Journal of Numerical Methods in Fluids*, Vol. 53, No. 8, 2007, pp. 1399–1422.
- [31] Eldredge, J. D., "Numerical Simulation of the Fluid Dynamics of 2D Rigid Body Motion with the Vortex Particle Method," *Journal of Computational Physics*, Vol. 221, No. 2, 2007, pp. 626–648. doi:10.1016/j.jcp.2006.06.038
- [32] Wang, Z. J., Birch, J. M., and Dickinson, M. H., "Unsteady Forces and Flows in Low Reynolds Number Hovering Flight: Two Dimensional Computations vs Robotic Wing Experiments," *Journal of Experimental Biology*, Vol. 207, Jan. 2004, pp. 449–460. doi:10.1242/jeb.00739
- [33] Mueller, T. H., *Fixed and Flapping Wing Aerodynamics for Micro Air Vehicles Applications*, AIAA, Reston, VA, 2001, pp. 232–246.
- [34] Shyy, W., Lian, Y., Tang, J., Viieru, D., and Liu, H., *Aerodynamics of Low Reynolds Number Flyers*, Cambridge Univ. Press, Cambridge, England, U.K., 2008, pp. 122–144.
- [35] Sane, S. P., "The Aerodynamics of Insect Flight," *Journal of Experimental Biology*, Vol. 206, Dec. 2003, pp. 4191–4208. doi:10.1242/jeb.00663
- [36] Wang, Z. J., "Dissecting Insect Flight," *Annual Review of Fluid Mechanics*, Vol. 37, Jan. 2005, pp. 183–210. doi:10.1146/annurev.fluid.36.050802.121940
- [37] Taha, H. E., Hajj, M. R., and Nayfeh, A. H., "Flight Dynamics and Control of Flapping-Wing MAVs: A Review," *Journal of Nonlinear Dynamics*, Vol. 70, No. 2, 2012, pp. 907–939. doi:10.1007/s11071-012-0529-5
- [38] Neef, M., and Hummel, D., "Euler Solution for a Finite-Span Flapping Wing," *Fixed and Flapping Wing Aerodynamics for Micro Air Vehicle Applications*, edited by Muller, T. J., Vol. 195, Progress in Astronautics and Aeronautics, AIAA, Reston, VA, 2001, pp. 429–449, Chap. 19.
- [39] Markow, T., and O'Grady, P., *Drosophila: A Guide to Species Identification and Use*, Academic Press, San Diego, CA, 2006, pp. 65–77.
- [40] Roccia, B. A., Preidikman, S., Massa, J. C., and Mook, D. T., "Development of a Kinematical Model to Study the Aerodynamics of Flapping-Wings," *International Journal of Micro Air Vehicles*, Vol. 3, No. 2, 2011, pp. 61–88. doi:10.1260/1756-8293.3.2.61
- [41] Chorin, A. J., *Vorticity and Turbulence*, Springer-Verlag, New York, 1994, pp. 9–12.
- [42] Van Garrel, A., "The Development of a Wind Turbine Aerodynamics Simulation Module," ECN Rept. ECN-C-03-079, Delft Univ. of Technology, Delft, The Netherlands, 2003.
- [43] Rusak, Z., Wasserstrom, E., and Seginer, A., "Numerical Calculations of Nonlinear Aerodynamics of Wing-Body Configurations," *AIAA Journal*, Vol. 21, No. 7, 1983, pp. 929–936. doi:10.2514/3.8179
- [44] Konstantinopoulos, P., Mook, D. T., and Nayfeh, A. H., "A Numerical Method for General Unsteady Aerodynamics," *AIAA Atmospheric Flight Mechanics Conference*, AIAA Paper 1981-1877, 1981.
- [45] Preidikman, S., "Numerical Simulations of Interactions Among Aerodynamics, Structural Dynamics, and Control Systems," Ph.D. Dissertation, Dept. of Engineering Science and Mechanics, Virginia Polytechnic Inst. and State Univ., Blacksburg, VA, 1998.
- [46] Preidikman, S., and Mook, D. T., "Time-Domain Simulations of Linear and Nonlinear Aeroelastic Behavior," *Journal of Vibration and Control*, Vol. 6, No. 8, 2000, pp. 1135–1175. doi:10.1177/107754630000600802
- [47] Mook, D. T., and Maddox, S. A., "Extension of a Vortex-Lattice Method to Include the Effects of Leading-Edge Separation," *Journal of Aircraft*, Vol. 11, No. 2, 1974, pp. 127–128. doi:10.2514/3.60336
- [48] Leroy, A., Bruon, F., and Devinant, P., "Unsteady Aerodynamic Model for Thin Wings with Evolutive Vortex Sheets," *Research and Technology Organisation (RTO) Applied Vehicle Technology Symposium on Advanced Flow Management: Part A — Vortex Flows and High Angle of Attack for Military Vehicles*, RTO Paper RTO-MP-069(I), Loen, Norway, 2001.
- [49] Sakurai, A., and Uchihori, H., "Unsteady Vortex Lattice Calculation of the Flow Around a Slender Delta Wing," *The Institute of Space and Astronautical Science Report*, Vol. 12, 1990, pp. 53–59.
- [50] Lighthill, M. J., "A New Approach to Thin Airfoil Theory," *Aeronautical Quarterly*, Vol. 3, 1951, pp. 193–210.
- [51] Ehlers, F. E., and Manro, M. E., "A Method for Computing the Leading-Edge Suction in a Higher-Order Panel Method," NASA CR-3730, 1984.
- [52] Kandil, O. A., Mook, D. T., and Nayfeh, A. H., "Nonlinear Prediction of the Aerodynamic Loads on Lifting Surfaces," *Journal of Aircraft*, Vol. 13, No. 1, 1976, pp. 22–28.
- [53] Birch, J. M., and Dickinson, M. H., "Spanwise Flow and the Attachment of the Leading-Edge Vortex on Insect Wings," *Nature (London)*, Vol. 412, Aug. 2001, pp. 729–733. doi:10.1038/35089071
- [54] Shyy, W., Berg, M., and Ljungqvist, D., "Flapping and Flexible Wings for Biological and Micro Air Vehicles," *Progress in Aerospace Sciences*, Vol. 35, No. 5, 1999, pp. 455–505. doi:10.1016/S0376-0421(98)00016-5
- [55] Rusak, Z., Wasserstrom, E., and Seginer, A., "Convergence Characteristics of a Vortex Lattice Method for Nonlinear Configuration Aerodynamics," *Journal of Aircraft*, Vol. 22, No. 9, 1985, pp. 743–749. doi:10.2514/3.45196
- [56] Fry, S. N., Sayaman, R., and Dickinson, M. H., "The Aerodynamics of Hovering Flight in *Drosophila*," *Journal of Experimental Biology*, Vol. 208, 2005, pp. 2303–2318. doi:10.1242/jeb.01612
- [57] Bos, F. M., Lentink, D., van Oudheusden, B. W., and Bijl, H., "Numerical Study of Kinematic Wing Models of Hovering Insect Flight," *45th AIAA Aerospace Sciences Meeting and Exhibit*, Reno, Nevada, AIAA Paper 2007-482, 2007.
- [58] Brodsky, A. K., *The Evolution of Insect Flight*, Oxford Univ. Press, New York, 1999, pp. 36–43.
- [59] Fry, S. N., Sayaman, R., and Dickinson, M. H., "The Aerodynamics of Free-Flight Maneuvers in *Drosophila*," *Science*, Vol. 300, 2003, pp. 495–498. doi:10.1126/science.1081944

- [60] Koumoutsakos, P., "Multiscale Flow Simulations Using Particles," *Annual Review of Fluid Mechanics*, Vol. 37, 2005, pp. 457–487.
doi:10.1146/annurev.fluid.37.061903.175753
- [61] Winckelmans, G. S., and Leonard, A., "Contributions to Vortex Particle Methods for the Computation of Three-Dimensional Incompressible Unsteady Flows," *Journal of Computational Physics*, Vol. 109, No. 2, 1993, pp. 247–273.
doi:10.1006/jcph.1993.1216
- [62] Greengard, L., and Rohklin, V., "A Fast Algorithm for Particle Simulations," *Journal of Computational Physics*, Vol. 135, No. 2, 1997, pp. 280–292.
doi:10.1006/jcph.1997.5706

R. Gordnier
Associate Editor